Stark Shifts and Ion-Ion Interaction in Europium Doped $YAlO_3$

- On the Road to Quantum Computing

Master's thesis
by
Markus Persson

Abstract

A new exciting branch of information technology is called quantum computing. In this field one tries to make use of the quantum mechanical properties of matter to enable computational performance and processes not achievable on a classical computer. The photon echo group at the Division of Atomic Physics, LTH, are pursuing a quantum computer concept using inorganic crystals doped with rare-earth-elements as the hardware.

The report will give a very brief general description of classical computers and an introduction to quantum computers. This is followed by the work done for my master's thesis, which involves characterisation of the $Eu^{3+} : YAlO_3$ crystal intended as quantum computer hardware, with the use of different optical techniques. The main task was to investigate how Eu^{3+} ions effect each other through dipole-dipole interaction by exciting ions which all have a permanent dipole moment in a specific direction. To accomplish this the possible directions of the dipole moments were obtained using Stark-modulated photon echoes. In order to study the ion-ion interaction using the technique describe in this report it is necessary to know how the absorption properties of the crystal alters when an electric field is applied. Such information was obtained by observing the Stark shifts of spectral holes burned into the absorption profile. Finally the report treats the experiments performed in order to detect the ion-ion interaction.

Contents

Chapter 1

Introduction

There are many different paths that science follow these days to find solutions on how to build faster computers. One can be summarised by the word *minia-turisation*. The goal is to construct smaller and smaller circuits, and to squeeze in as many transistors as possible in as little space as possible. This leads to shorter distances for the electric signals to travel and therefor a faster flow of information. This ambition is a great part of the modern research field of nanotechnology, where the name hints at the physical dimensions. A second and exciting path towards faster computation is the quantum computer, which also could make previously unsolvable operations possible. The construction of hardware for a quantum computer has been the main purpose of my thesis.

1.1 Classical computers

If Moore's law continues to be a valid description of reality, the microprocessors should double their computation speed every 18 months. To accomplish this circuits presumably must shrink in size at the same pace. This means that a transistor will only consist of a few atoms in a decade or two. However, the technology of today already permits manipulation of single electrons with precision. It is possible to "pick up" and move an electron from a non-conducting area to an island of a semiconductive material, which then also will become non-conducting. The transferred electron will block the way for other electrons due to the relatively strong repelling Coulomb force. This scheme could evolve into a small transistor in the future [1].

When structures with dimensions on the nanometer scale are created, quantum mechanical effects can be significant and must be considered in order to predict the consequences of different events. In spite of this, the new smaller circuits will work in a similar way as their larger predecessors, using electrical currents as transport for the information which is in the form of bits. A bit can either have the value "0" or "1". Thus, there is no fundamental difference in comparison to the computers of today.

1.2 The quantum computer

1.2.1 What is a quantum computer?

The differences between a quantum computer and a classical computer are large, but so are the similarities. Just as in a classical computer, the information is stored in bits, called qubits in a quantum computer. The difference is the way the qubits are represented, e.g. as different quantum states in an atom or an ion. Two different states are used to symbolise "0" and "1" as qubit values, using exactly the same principle as in the ordinary computer. In Dirac-notation[1] these states are denoted $|0\rangle$ and $|1\rangle$. A quantum mechanical system can be completely described by its state, which can be symbolised by $|\psi\rangle$.

The main difference from a classical computer is that a quantum computer makes use of the ability of a quantum mechanical system to be in a coherent[2] superposition of different states:

$$|\psi\rangle = \sum_n c_n e^{i\chi_n} |\phi_n\rangle \qquad (1.1)$$

with

$$\sum_n |c_n|^2 = 1, \qquad (1.2)$$

where $|\psi\rangle$ represents the state of the system and $|c_n|^2$ is the probability of observing the system in state ϕ_n. Henceforth the notation $|n\rangle$ will be used instead of ϕ_n. Due to the superposition properties, a qubit can be in an unlimited number of different superposition states, even though only two quantum states are used, the $|0\rangle$ and $|1\rangle$. An example with energies follows: If two eigenstates with the corresponding energy eigenvalues E_0 and E_1 are used as qubit states, the particle in question have an equal probability of possessing all superpositions of E_0 and E_1. Not until the energy of the particle is measured it collapses into either the energy E_0 or E_1. Thanks to this property, using superpositions of states, a quantum computer can work with several computations at the same time when the system is not collapsed. This is called "quantum parallelism" and is characteristic for a quantum computer. To read more about this field see [1] and the more detailed [2].

To build a quantum computer for practical use, one must construct multi-qubit logic gates, where the evolution of one qubit depends on the states of other qubits. If two or more qubits show this property they can be *entangled*. An example of an entangled state follows: Consider a 0-spin particle decaying into two $\frac{1}{2}$-spin particles. In order to conserve the angular momentum of the system the emitted particles must have spins in opposite directions. If no action is taken to distinguish the particles from each other, the resulting quantum state is

$$|\psi\rangle_{12} = \frac{1}{\sqrt{2}}(|\uparrow\rangle_1 |\downarrow\rangle_2 + e^{i\chi} |\downarrow\rangle_1 |\uparrow\rangle_2), \qquad (1.3)$$

where $|\downarrow\rangle_2$ means particle 2 with spin down. If the phase $i\chi$ is well-defined, the two states are said to be *quantum coherent*. This coherence is very important when performing qubit manipulations and photon echoes.

---

[1] A practical notation when representing states in quantum mechanics [8]
[2] The phase $i\chi_n$ between the different states ϕ_n is well-defined

In the above state there is no way of saying, without measuring, what value (↑ or ↓) the spin of particle 1 has. The situation is exactly the same for particle 2. Even so, if one of the particles is measured on, the other particle immediately assumes a specific state, which has the opposite spin to that of the measured particle. This phenomenon is not dependent on the spatial distance between the particles when measured. In this example the total state $|\psi\rangle_{12}$ can not be totally described by one of the particles individually. This means the total state can not be factorised into a direct product of the states of the two particles. This is the definition of entanglement.

As a conclusion one could say that the difference between a classical computer and a quantum computer is the latters' ability to use:

1. quantum parallelism

2. entanglement

1.2.2 The advantages of a quantum computer

Quantum computers are not ment to be a way of increasing the speed of today's computation processes using quantum mechanical effects. Greater computation speeds will instead be accomplished by the utilisation of new algorithms, which could not be executed on a classical digital computer.

One example of such an algorithm became known in 1994 when Peter Shor published a theory [3] regarding factorisation of large integers into their prime number components. The computation complexity was said to scale polynomially with the length of the integer, instead of exponentially as on a classical computer. This means that an integer, too large to be factorised on a classical computer in feasible time, could now be just that with the use of a quantum computer. The reason why this is so interesting is that most of modern commercial and military cryptography uses the fact that factorisation of very large integers into their prime number components can *not* be done in practise.

Two years later (1996) Lov K. Grover, a scientist at American Bell Labs, published a new promising algorithm [4], specially made for quantum computers. The benefit of the algorithm can appear more obvious than of Shor's ditto. Grover's algorithm was said to be able to find a given element in an unsorted database of size N, by the use of only $\sqrt{N}$ computations. A classical computer typically needs $N/2$ operations on average to find the element. This would mean that Grover's algorithm only needs 1 000 operations to find an element in a database consisting of 1 000 000 elements, instead of 500 000.

The possibility of rapid computation motivates quantum computing from an applications point of view. From the view of pure science it is for example interesting to develop quantum systems where you in detail can control the complete quantum mechanical wavefunction and in this way explore the non-classical world.

6

Chapter 2

Quantum computer concepts

Today there are several schemes for quantum computers, which either show promising results or are already able to perform actual computations. There actually exist working quantum computers which have demonstrated as much as a 7-bit logic operation in science labs [5]. The following three techniques have either been selected for their splendid results or for a concept close to the scheme used by our group. They all have two fundamental properties, the ability of qubit construction and a feasible interaction mechanism between qubits, which makes entanglement possible.

2.1 Ion traps

The first system that was used to create logic gates for quantum computers was laser-cooled ions in an ion trap [2]. The ion trap consists of a cleverly constructed electric field, in which the charged ions feel a restoring force in the opposite direction of any movement. The low temperature of the sample helps preventing disturbing thermal vibrations, which can change the quantum states of the ions. To reach sufficiently low temperatures, one utilises the technique of laser-cooling [6]. The whole system also depends on high vacuum to work. To manipulate the ions, which are placed in a line, a laser that can be directed to any individual ion is used. For the two qubit states $|\,0\,\rangle$ and $|\,1\,\rangle$, the energy ground state and a metastable excited state of the ions are used. The ions interact with each other through vibrations. One advantage of the ion trap approach is the isolation of the system from the surroundings.

2.2 Nuclear magnetic resonance

The most successful quantum computer schemes have been the nuclear magnetic resonance (NMR) based techniques [2]. One reason is that the creation of a qubit is fairly uncomplicated. One simply makes use of the natural two-level system[1] that the spin states of a spin-$\frac{1}{2}$ nucleus provide. In the magnetic field in an

---

[1]Spin up $(+\frac{1}{2})$ and spin down $(-\frac{1}{2})$

NMR machine, the degeneracy of the states is lifted. Another property that can act as an advantage is the non-uniqueness of the qubits. One qubit is not made up of one particle but of all particles with a certain absorption frequency in the whole ensemble. Typically you could use a liquid consisting of only one kind of molecule. Every atom in the molecules will have a specific absorption frequency, different from the others due to individual chemical surroundings. Thus, a liquid consisting of N-atom molecules could act as an N-qubit system. When the RF coils of the NMR machine induces a spin transition of an atom, the other atoms in the molecule experience a different electromagnetic surrounding and shifts their resonance frequencies. In this way the atoms interact.

2.3 Quantum dots

One approach to constructing a quantum computer is based on the properties of quantum dots, described in [7]. A quantum dot can be seen as a potential well in three dimensions, in which an electron can possess discrete energy values. Some aspects of this technique resembles the solution we have chosen for the future construction of a quantum computer. A basic system would consist of two quantum dots, separated by a distance L, with one electron confined in each. In an applied electric field the charge density in the dots will be spatially shifted, and a dipole moment is then induced in each dot. The dipole moment of the ground state $|0\rangle$ is not parallel to the dipole moment of the excited state $|1\rangle$. When one of the dots is excited $|0\rangle \longrightarrow |1\rangle$ the absorption frequency of the other dot is shifted due to the changed electric field from the excited dot. This can be used to perform logic gate operations.

Chapter 3

The $Eu^{3+} : YAlO_3$ quantum computer

Our group has developed an idea on how to generate interacting qubits in solid materials, which normally is difficult. The system consists of inorganic crystals doped with rare-earth ions kept at cryogenic temperatures [9]. In this case the system is europium doped into yttrium-aluminate ($Eu^{3+} : YAlO_3$). Two hyperfine levels of the ground state in Eu^{3+} are utilised as qubit states $|0\rangle$ and $|1\rangle$. To be able to perform population transfers between these two states, a third excited state $|exc\rangle$ is also needed. The transitions $|0\rangle \longleftrightarrow |exc\rangle$ and $|1\rangle \longleftrightarrow |exc\rangle$ represent the corresponding $^7F_0 - {^5D_0}$ (581,68 nm) transition of the Eu^{3+} ions in $YAlO_3$. The levels in Figure 3.1 corresponds to the following atomic states:

- $|exc\rangle = {^5D_0}$
- $|0\rangle = {^7F_{0,\pm\frac{1}{2}}}$
- $|1\rangle = {^7F_{0,\pm\frac{3}{2}}}$
- $|aux\rangle = {^7F_{0,\pm\frac{5}{2}}}$

The last index determines the nuclear spin projection of the Eu^{3+} ion in the crystal, indicating that the ground state levels are doubly degenerate. The first lower index is the spin-orbit interaction J of the system as in ordinary LS-terminology. One reason for using this specific material is the relatively long optical coherence time of the system, which is approximately 250 μs [11] for the $^7F_0 - {^5D_0}$ transition. All quantum algorithms are said to require quantum coherence and entanglement to operate. This "long" coherence time makes it possible, in theory, to compute hundreds of operations before the system must be prepared again.

Another reason for using $Eu^{3+} : YAlO_3$ is the long lifetimes of the hyperfine levels of many hours, which has been obseved by e.g. our group. This makes the initial qubit construction process easier as this then in practice can be done without any time constraint.

A third reason for using europium doped $YAlO_3$ are the very special absorption properties of the europium ions, and rare-earths in general, described in section 3.1.1.
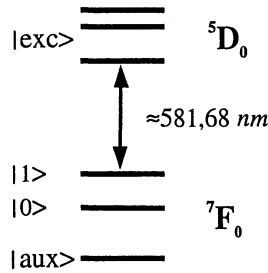
|exc> ≡ $^5D_0$

≈581,68 nm

|1> —

|0> — $^7F_0$

|aux> —

Figure 3.1: Energy level diagram showing the important states for the quantum computing scheme. The excited state consists of all levels in the $^5D_0$ manifold. The auxiliary level is used in the qubit construction process.

3.1 Rare-earth-ions

The ions of the rare-earth elements all have similar chemical and optical properties. This arises from their unusual electronic configuration. All the elements have the same number of electrons in the outer filled shells, that is to say $5s^2p^6$. The only difference between the elements is the number of electrons in the inner $4f$ shell. The shielding of the $4f$ shell by the outer $5s$ and $5p$ electrons has the result that the rare-earths have very narrow $4f - 4f$ transition linewidths, also when doped into a crystal. The linewidths are otherwise broadened by lattice interaction, and are still so to some extent.

3.1.1 Absorption profile

Due to the shielding of the $4f$ electrons, the absorption profile of Eu^{3+} will have very special properties. Every ion will have a very sharp $^7F_0 - ^5D_0$ transition with a homogeneous[1] broadening of about 1 kHz [10] [11]. When the Eu^{3+} ions are doped into the $YAlO_3$ crystal they will all aquire a shift in their $^7F_0 - ^5D_0$ absorption frequency. The shift depends strongly on the surroundig electric field. Because of lattice imperfections the local electric field varies for the different ions, causing an inhomogeneously[2] broadened absorption profile of around 5 GHz [10] for the entire crystal.
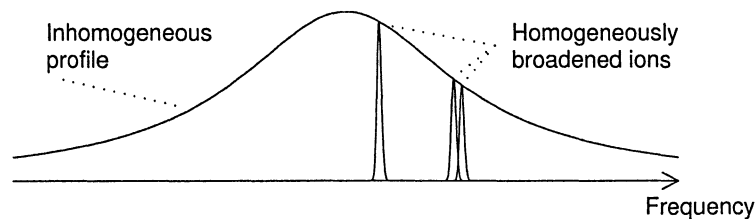

Figure 3.2: Inhomogeneous and homogeneous broadening

---

[1] In homogeneous broadening all ions are equally affected
[2] In inhomogeneous broadening the ions are not equally affected

This combination of a very narrow homogeneous line-width and a relatively large inhomogeneous broadening (see Figure 3.2) is very favourable when it comes to creating multiple qubits. It gives the possibility to address many very narrow individual frequency channels within a large frequency interval. The ratio between the homogeneous broadening of ≈ 1 kHz and the inhomogeneous broadening of ≈ 5 GHz indicates a number of $\approx 10^7$ different channels to work with. Although it is not clear how many frequency channels one qubit practically needs as a minimum, it is safe to say the possibilities are good.

3.2 Laser-induced frequency shifts

In order to perform multi-qubit operations, coupling between the different ions is necessary. Multi-qubit operations are also called *controlled logic* which is a corner stone in quantum algorithms.

3.2.1 Ion-ion interaction

One way of creating the coupling needed, is to use the fact that Eu^{3+} has different permanent electric dipole moments in the $^7F_0$ ground state and the $^5D_0$ excited state when doped into a crystal. The dipole moment in the excited state is larger and is oriented in the same direction as in the ground state. Here called $\bar{\mu}_g$ (g for *ground*) and $\bar{\mu}_e$ (e for *excited*). The electric field from each ion,
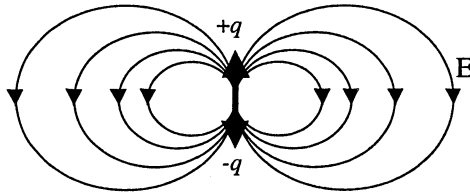

Figure 3.3: The electric field from an electric dipole

due to the dipole moment (see Figure 3.3), will change if it undergoes a transition from the ground to the excited state, or vice versa. It will become more intense or weaker respectively. As mentioned above, the transition frequencies of the ions are strongly dependent on the surrounding electric field. When one ion then is excited, it will shift the absorption frequency of all other ions close enough in space to be affected by the different electric field. The shift in absorption frequency D from the original frequency ν_{0i} for ion i when affected by the change in electric field from ion j is given by [9]

$$D_{ij} = \frac{(\Delta\mu_i)(\Delta\mu_j)}{4\pi h\epsilon_0\epsilon_r r_{ij}^3}[(\hat{\mu}_i \cdot \hat{\mu}_j) - 3(\hat{\mu}_i \cdot \hat{r})(\hat{\mu}_j \cdot \hat{r})] \qquad (3.1)$$

$$\nu_i = \nu_{0i} + D_{ij} \qquad (3.2)$$

where $\Delta\mu = |\bar{\mu}_e - \bar{\mu}_g|$, h is Planck's constant and r_{ij} is the distance between ion i and j. $\hat{\mu}$ and $\hat{r}$ are unit vectors along $(\bar{\mu}_e - \bar{\mu}_g)$ and $\bar{r}_{ij}$. For Eu in $YAlO_3$ $\Delta\mu \approx 3 \cdot 10^{-31}$ Cm according to[3] [13]. If ion j was the only ion affecting ion i

---

[3]The unit Cm reads Coulomb·meter

this would imply a shift in transition frequency of 1 GHz, 1 MHz and 1 kHz for the distances 1 nm, 10 nm and 100 nm between the ions respectively [9]. The situation in reality is somewhat more complicated.

An ion is affected by *every* ion in the crystal in some way. From equation (3.1) we know that the effect goes as $\frac{1}{r^3}$. This would make the effective volume, in which the affected ion is situated in the middle, fairly small. The pertubations from ions outside this volume can be neglected. Also, ions can have their dipole moments in opposite directions, cancelling some of the effect. This is not all. There is a third and fourth direction as well. They are antiparallel with respect to each other, and make an angle of approximately 28° [19] to the other two directions (shown in Figure 3.4). While conducting controlled logic, the
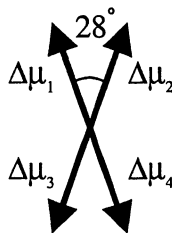

Figure 3.4: Possible directions of the permanent dipole moment.

frequency channels (possible qubits) must control each other, as stated above. It is important to know the shift of the ions in one channel, C_1, when exciting another, C_2, in order to prepare the qubits. This is not trivial. The ions in channel C_1 all, in principle, get shifted by a different magnitude. This is due to the different distances to the excited ions in the crystal. Members of C_1 sitting close to a C_2 ion will be shifted a lot, while ions far from all excited C_2 particles in space essentially will not be shifted at all. One way of enhancing the interacting effects could be to excite ions with electric dipole moment in one direction only (see Figure 3.5). In this way the fields from excited ions should interfere in a more constructive way, not cancelling each other to the same extent. Investigations of this effect are described in Chapter 9.

3.3   Controlled logic

In order to perform the logic operations in a controlled manner the qubits must be prepared before use. Ions of a qubit that interact weakly, or not at all, with the other qubits must be "eliminated". This can be done in the following way.

3.3.1   Preparing a qubit

The first action to take is to put all the C_1 ions used for the qubit in the same state, e.g. $|\,0\,\rangle$. By using optical pumping this is possible. The system is then said to be in a *pure* state. Secondly perform the excitation of the ions in channel C_2. If a laser now illuminates the crystal at frequency ν_{01}, all ions in C_1 not shifted sufficiently will absorb the light. They can now be easily moved to an auxiliary state using optical pumping. The auxiliary state $|\,aux\,\rangle$ is, in this case,
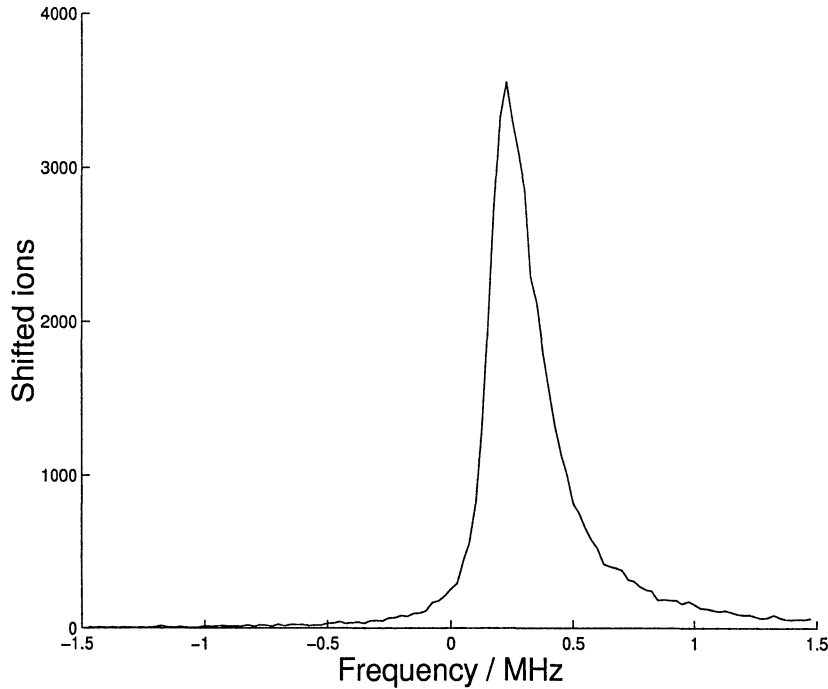
Figure 3.5: Theoretical distribution of the shifts in absorption frequencies of C_1 ions when exciting ions in a 40 MHz wide interval with their dipole moments in one direction only.

the third hyperfine level of the ground state (see Figure 3.1). The excited C_2 ions can now be driven back to the ground state by a laser pulse. The part of C_1 that was perturbed in frequency will now shift back to ν_{01}. If the same procedure is conducted again, but with C_1 as the controlling and C_2 as the target channel, the two channels will finally be able to control each other in an orderly fashion. It is n... in principle possible to perform controlled logic with C_1 and C_2 acting as two qubits.

3.3.2   The Controlled-NOT gate

Maybe the most simple, and therefor most discussed (and important), of the multi-qubit operations is the *Controlled-NOT* gate $(C - NOT)$. The essence of the $C - NOT$ gate is that the value of one qubit, called the target, is switched only if the control qubit has the logic value of "1". The value of the control qubit does not change. The possible inputs and the corresponding results can most simply be descibed by the following table:

$$|0\rangle_c|0\rangle_t \longrightarrow |0\rangle_c|0\rangle_t \qquad |0\rangle_c|1\rangle_t \longrightarrow |0\rangle_c|1\rangle_t$$
$$|1\rangle_c|0\rangle_t \longrightarrow |1\rangle_c|1\rangle_t \qquad |1\rangle_c|1\rangle_t \longrightarrow |1\rangle_c|0\rangle_t$$

where $|n\rangle_c$ refer to the control qubit and $|n\rangle_t$ refer to the target qubit. To use *quantum parallelism* effects the qubits now have to be in a superposition of $|0\rangle$ and $|1\rangle$ before the operation is conducted.

13

To do the *C-NOT* in practice first prepare two qubits, then generate appropriate laser pulses[4] with frequencies corresponding to the following transitions:

1. $|0\rangle_c \longleftrightarrow |exc\rangle_c$

2. $|0\rangle_t \longleftrightarrow |exc\rangle_t$

3. $|1\rangle_t \longleftrightarrow |exc\rangle_t$

4. $|0\rangle_t \longleftrightarrow |exc\rangle_t$

5. $|0\rangle_c \longleftrightarrow |exc\rangle_c$

If the control qubit starts out in its $|0\rangle$ state, the target qubit will be shifted out of resonance by the ion-ion interaction after step 1. If this is the case steps 2 to 4 will not effect the ions of the target qubit. On the other hand if the control qubit starts out in $|1\rangle$ the control ions will not be excited by step 1. If then the target qubit is in state $|0\rangle$ it will first be put in $|exc\rangle$ by step 2 and then driven down to $|1\rangle$ by step 3 (stimulated emission). If the target qubit instead starts out in $|1\rangle$, steps 3 and 4 will transfer it to the $|0\rangle$ state, i.e. the state of the target qubit is shifted.

The scheme described above is called a $C^1 - NOT$ gate. It can be extended into a $C^n - NOT$ gate by repeating steps 1 and 5 for all n control qubits.

---

[4] π-pulses, driving the transition from one state to the other with a probability equal to 1

Chapter 4

Photon echoes

Writing a master's thesis in the photon echo group, one simply must conduct some photon echo experiments. As a matter of fact, photon echoes are very powerful when it comes to examining small energy splittings and fine structures in a crystal. When it comes to exciting Eu^{3+} ions and create ion-ion interaction, I have chosen a technique that will only excite the ions with their dipole moment in a specific direction. This is to maximise the frequency shifts by minimising cancellation of electric fields between excited ions. To achieve this selectivity one has to know the directions of the dipole moments with respect to an applied electrical field. This can be determined with the help of *Stark-modulated photon echoes* (SMPE), described in section 4.2.

4.1 Theory of photon echoes

When an ensemble of atoms radiate after an excitation, the intensity usually decays exponentially. The temporal signature of the emission can however be significantly different if the atoms are prepared in the right way. Consider the electric field emitted from a single decaying atom

$$E(t) = E_0 e^{-i\omega t} \tag{4.1}$$

where ω corresponds to the energy difference between the two energy levels involved. If we now consider all ions with the total absorption frequency distribution $G(\omega)$, representing the inhomogeneous absorption profile of $Eu^{3+} : YAlO_3$, we get

$$E(t) = E_0 \int G(\omega) e^{-i\omega t} d\omega \tag{4.2}$$

As we can se from equation 4.2 $E(t)$ is the temporal Fourier transform of the absorption frequency distribution $G(\omega)$. This implies that we can make the ions emit any temporal signal we want. This can be achieved just by suitably preparing the distribution of frequencies $G(\omega)$ and then making the ions radiate at the same time.

This preparation of $G(\omega)$ is feasible thanks to the ability of the ions to be in a coherent superposition of states. The single-electron wavefunctions of the

ground and excited states can be written as

$$\psi_g(\bar{r}, t) = \phi_g(\bar{r})e^{-i\omega_g t}$$
$$\psi_e(\bar{r}, t) = \phi_e(\bar{r})e^{-i\omega_e t} \tag{4.3}$$

where ω_g and ω_e are the frequencies corresponding to the energies[1] of the ground and excited states. The wavefunction of an ion in a superposition of these states is

$$\psi_{tot} = c_g\psi_g + c_e\psi_e \tag{4.4}$$

where c_n can be complex numbers. The probability of detecting an electron in a given position $\bar{r}$ is given by $|\psi_{tot}|^2$ and the following charge density is $-e|\psi_{tot}|^2$. An ion with wavefunction ψ_{tot} will then have a charge density oscillating at the frequency $\omega_e - \omega_g$ according to

$$|\psi_{tot}|^2 = \psi_{tot} \cdot \psi_{tot}^*$$

$$(\phi_g e^{-i\omega_g t} + \phi_e e^{-i\omega_e t}) \cdot (\phi_g e^{-i\omega_g t} + \phi_e e^{-i\omega_e t})^*$$
$$= \phi_g^2 + \phi_e^2 + 2\phi_g\phi_e \cos\left((\omega_e - \omega_g)t\right) \tag{4.5}$$

This is equal to the transition frequency between the ground and excited states. As in an antenna, electrons in accelerated motion radiates and thus an ion in a superposition of states emits radiation.

If an ion in a superposition is irradiated by a short laser pulse, the outgoing light can be described as interference between the radiation emitted by the ion and the laser light. The relative phase of the two fields will determine whether absorption or stimulated emission occur. If the two fields are out of phase they cancel each other and we interpret it as absorption. If they are in phase, the outcoming field will be larger than the incoming and we have stimulated emission.

We now set many ions in a superposition of the ground and excited states by using a very short laser pulse, wide enough in frequency to cover a large part of the inhomogeneous absorption profile. They will then radiate with a lot of different frequencies, starting in phase but spreading out to a random phase distribution very quickly. The next step is to send in another short pulse after the time $T = t_2 - t_1$ (see Figure 4.2). If ions with an oscillation frequency ω_1 are in phase with the second pulse, they will be excited and in the same way ions out of phase with a frequency ω_2 will be de-excited. In fact, not only ions with frequencies ω_1 and ω_2 are affected. All ions with a frequency ω fulfilling $\omega T = \omega_1 T + 2\pi n$, where n is an integer, will be excited and all ions satisfying $\omega T = \omega_2 T + 2\pi n$ will be de-excited. This will create a periodic structure in the populations of the excited and ground states which is illustrated in Figure 4.1. The structure will have a period of $1/T$ in the frequency plane as expected. The longer the time between the pulses the shorter the period will become. Thus the structures contain the Fourier contents of the electric field effecting the ions from the time they were set in a superposition by the first pulse to the end of the second pulse.

---

[1] $E = \hbar\omega$

After first pulse   **After second pulse**

Upper
state

Lower
state

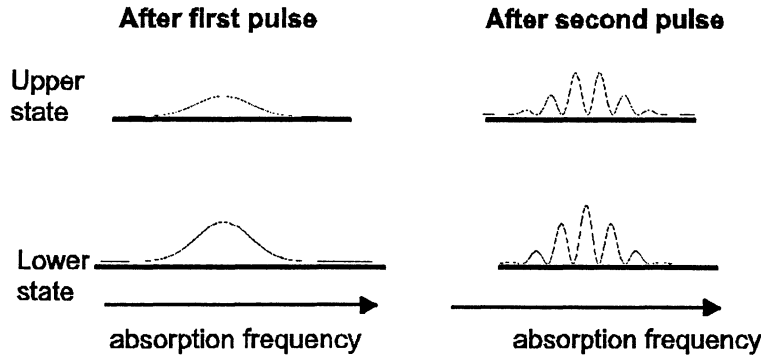absorption frequency   absorption frequency

Figure 4.1: The frequency-dependent populations created by the first two light pulses in a three pulse photon echo construction

When this creation of $G(\omega)$ is done, the last thing to do is to send in a final third laser pulse (see Figure 4.2) to put the ions in a superposition again. Their emitted radiation, with the frequency distribution $G(\omega)$, will be in phase after the time $T = t_3 + (t_2 - t_1)$ and a light pulse will appear, seemingly from nowhere. This is the photon echo. The method described here is called a three-pulse photon echo. If the time between pulse two and three is set to zero the process is exactly the same and we still get an echo as before, but now with the use of only two pulses. This is the method used in this project and is called a two-pulse photon echo (*2PPE*).
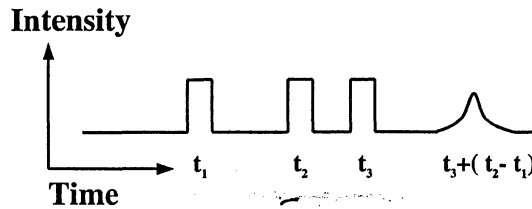
Intensity

Time t_1 t_2 t_3 $t_3+(t_2-t_1)$

Figure 4.2: Laser pulse sequence for construction of a photon echo. The pulses at t_1, t_2 and t_3 are laser pulses. The resulting echo appears after the time $t_3 + (t_2 - t_1)$.

4.2   Stark-modulated photon echoes

If an electric field is applied to an electric dipole, the dipole will feel a force trying to orient it in the direction of the field. If the dipole is prevented from moving, e.g. in a crystal, it will gain in potential energy according to

$$\Delta V = \bar{\mu} \cdot \bar{E}. \tag{4.6}$$

If an atom has a permanent dipole moment which has different magnitudes in the ground and excited states of the atom and an electric field is present, the

energy levels are Stark-shifted. The transition frequency will then change as

$$\Delta\Omega = \frac{\Delta\bar{\mu} \cdot \bar{E}}{\hbar}.\tag{4.7}$$

If the electric field is applied between t_1 and t_2 in the photon echo construction, ions with a positive value of equation[2] 4.7 will "gain" an amount of $\Delta\Omega \cdot \tau_E$ in phase, where τ_E is the duration of the E-field pulse. If the product $\Delta\bar{\mu} \cdot \bar{E}$ is negative[3] the ions will "loose" in phase. This property will effect the photon echo intensity if the system used as echo material includes ions with more than one value of $\Delta\bar{\mu} \cdot \bar{E}$. One can then treat the two, or more, ensembles of ions separately, producing one photon echo each. The phase factors $\Delta\Omega \cdot \tau_E$ are different for the ensembles and results in echoes that will have a mutual phase difference of

$$(\Delta\Omega_1 - \Delta\Omega_2)\tau_E = \pi n$$

in the case of two ensembles. This results in a maximum if $n = even$ and a minimum if $n = odd$. If different photon echoes are produced with increasing τ_E, the echo intensities will vary as

$$I_{echo}(\tau_E) \propto |cos((\Delta\Omega_1 - \Delta\Omega_2)\tau_E)|^2\tag{4.8}$$

when the echoes from two different ensembles successively comes in and out of phase. This can be generalised into any number of different ensembles, all individually resulting in one echo interfering with every other echo, thus creating a modulation. According to this, atoms with three different energy shifts, i.e. three ensembles, will produce a modulation with three frequencies[4] and so on. An investigation of Stark-modulated photon echoes is presented in Chapter 7.

4.2.1 Alternative explanation of SMPE

A commonly used pictorial explanation of the photon echo process is to view it as a $10\,000\ m$ race. The first pulse in the echo construction is equal to the starter firing the gun at the start of the race. As the race goes on the runners will spread out on the track. The speed of a runner correspond to the oscillation frequency in the superposition created by pulse one. The distance run on the track represents the accumulated phase of the oscillation. The second pulse in a 2PPE is equal to telling the runners to turn around and run in the other direction on the track. When they return to the start line they all arrive at the same time, since the fast runners have caught up with the slower ones. This resembles the oscillations of the ions coming into phase with each other again, resulting in an echo.

When the electric field is applied during a SMPE, the ions are divided into groups retrieving a different amount of energy and therefor different amounts of phase contribution. This can be seen as runners from different groups running faster or slower during the time of the E-field pulse. When they later turn around and run the other way, runners within a group will cath up to each other at the same time as all other groups but at different places on the track. This represents the interfering echoes with different phases.

---

[2]The projection of $\bar{\mu}$ on $\bar{E}$ is parallel to $\bar{E}$

[3]The projection of $\bar{\mu}$ on $\bar{E}$ is anti-parallel to $\bar{E}$

[4]$I_{echo}(\tau_E) \propto |cos((\Delta\Omega_1 - \Delta\Omega_2)\tau_E) + cos((\Delta\Omega_1 - \Delta\Omega_3)\tau_E) + cos((\Delta\Omega_2 - \Delta\Omega_3)\tau_E)$

Chapter 5

Spectral holeburning

Both the $^7F_0$ and the $^5D_0$ state of Eu^{3+} in $YAlO_3$ consist of three doubly degenerate hyperfine levels. When a transition from a level in the ground state to another level in the excited state is induced, the atom stay excited for a millisecond or so. When it relaxes it can end up in either of the three levels in the ground state. If atoms are continously excited at the same transition frequency, a depletion of atoms in the initial level will occur. This shows up as a "hole" in an absorption measurement at the given transition frequency. Transitions from the initial level to the other two excited levels will be less likely now, resulting in two more holes, called "side-holes". Since the atoms are depleted from the initial level they are collected in the other two ground state hyperfine levels. As a result, transitions from these two levels will be more likely, showing as peaks ("anti-holes") in an absorption measurement. Due to the inhomogeneous
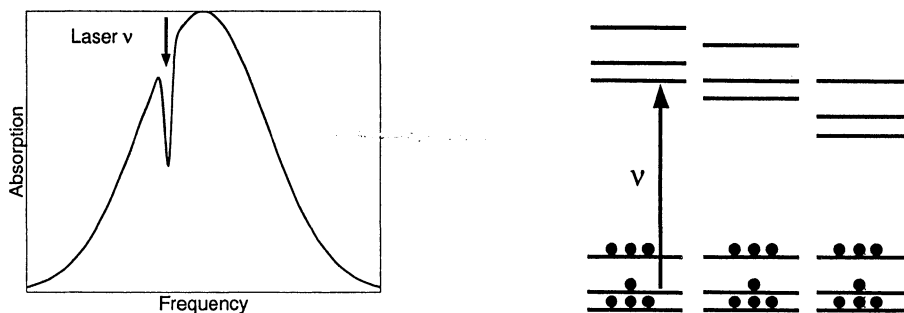
Figure 5.1: Hyperfine holeburning at frequency ν in an inhomogeneously broadened material like $Eu^{3+}:YAlO_3$.

broadening in the crystal, there are nine different transitions from the ground to the excited state corresponding to the same transition frequency, some of them shown in Figure 5.1. This will result in a somewhat complicated structure of the absorption profile when one single hole is "burnt". All in all, with two isotopes (see section 6.7) this results in 12 side-holes and 84 anti-holes [10]. This is pictured in Figure 5.2.
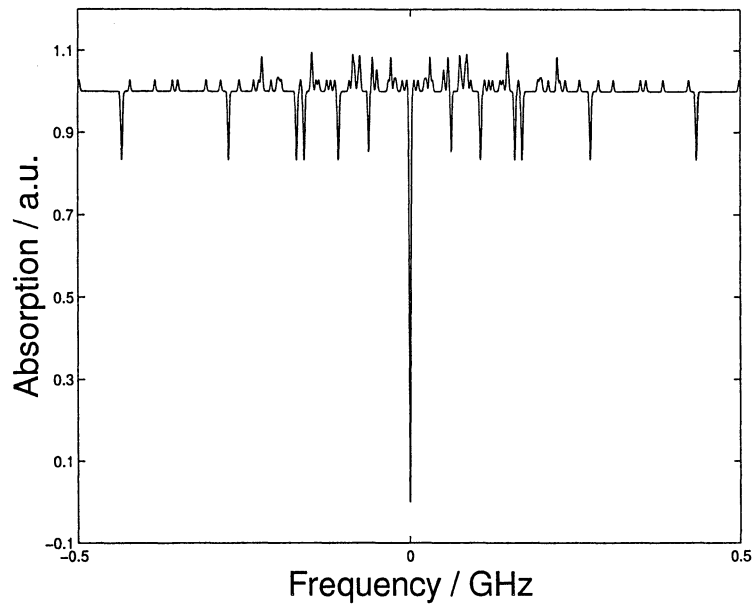
Figure 5.2: A theoretical calculation of the resulting absorption spectrum, after burning a spectral hole.

5.1 Spectral holesplitting

When an electric field is applied to a crystal containing a spectral hole, the hole will start to broaden. Exactly as in SMPE, ions with different directions of their dipole moments will receive a different amount of change in absorption frequency when influenced by an applied electric field. If the field is increased further, and two different ensembles of ions are present, the broadened hole will split in two (shown in Figure 5.3). If there are more groups of ions with different energy shifts the hole will split up in as many components.

Total absorption

Absorption frequency
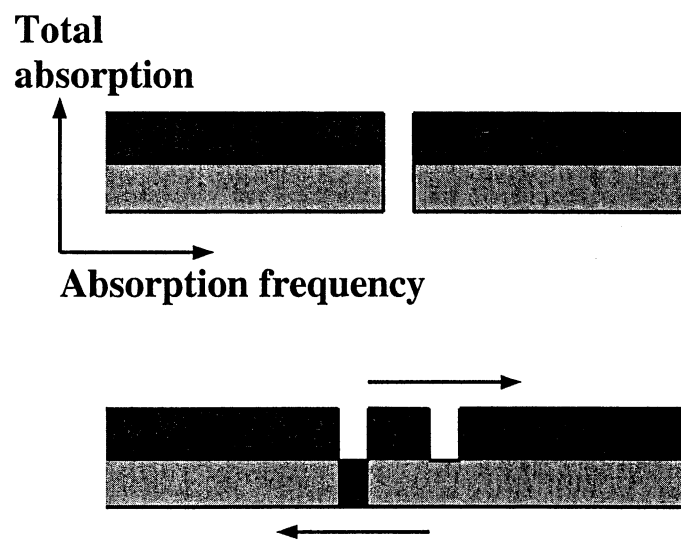
Figure 5.3: When an electric field is applied to a spectral hole (above) in a crystal with groups of ions with two different energy shifts, the hole will be split into two components (bottom) both having 50 % of the original absorption. The two groups of ions are represented by different colors.

Chapter 6

Equipment

6.1 Laser system

All experiments were conducted with a *Coherent CR-699-21* ring dye laser, pumped by a *Coherent Innova 400 Ar$^+$*-ion laser. The dye used was *Rhodamine 6G*, resulting in approximately $300mW$ output power. A schematic drawing of the dye laser cavity is given in Figure 6.1. An external wavelength meter was needed to measure the laser wavelength [15]. For stabilisation of the laser
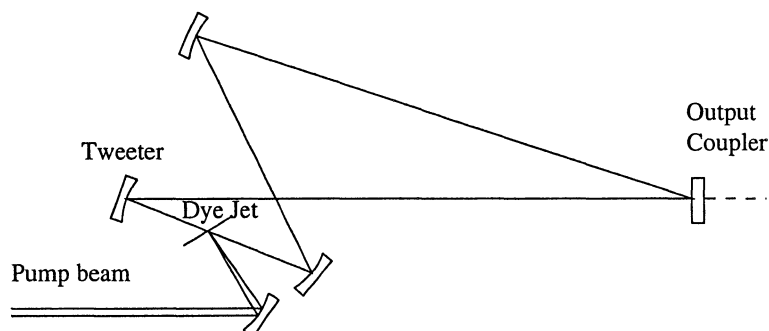
Figure 6.1: Description of the dye laser cavity, showing the basic structure.

frequency the laser uses an active servo system. The cavity can be adjusted in length by tilting a plate, at near Brewster angle, close to the output coupler, called the "woofer". The cavity length can also be altered by adjusting a high-frequency piezoelectric mounted mirror, called the "tweeter" (shown in Figure 6.1). The "woofer" provide large-scale and low-frequency jitter corrections, and the "tweeter" prevents high-frequency jitter with a 10 kHz bandwidth. The terms "woofer" and "tweeter" comes from the hi-fi equivalents.

An error signal that is used to feed the servo system is generated in a Fabry-Perot interferometer. A small part of the laser light is directed into this reference cavity immediately after exiting the dye laser. The interferometer has a transmission that varies repetitively with the frequency of the laser light. The error signal has its normalising point half way up a maximum where the derivative is

at max. A deviation from this point causes a positive or negative error output. The servo system gives the laser a linewidth of approximately 1 MHz.

On a larger time scale the frequency drift is much larger. This is due to temperature variations in the optical components of the laser and in the reference cavity. According to [16] this drift is less than 100 MHz/h. In Figure 6.2 one can se that the drift in practice can be somewhat smaller.
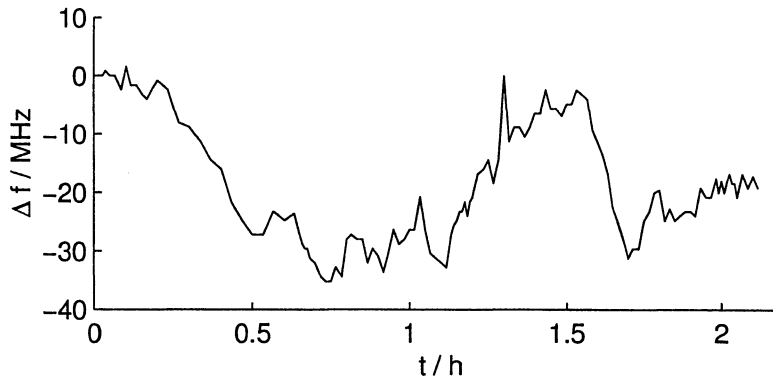

Figure 6.2: The laser frequency is registered once a minute in reference to a spectral hole. This plot of the drift is taken from [14].

6.2 Acousto-optic modulators

Acousto-optic modulators *(AOMs)* are used in laser experiments for electronic control of the intensity and direction of the laser beam. Acousto-optic interaction occurs in all optical media when an acoustic wave and a laser beam are simultaneously present. In an AOM an acoustic wave is launched into an optical medium perpendicular to the incoming light. In the medium it then generates a refractive index wave that behaves like a travelling sinusoidal grating for the laser light. An incident laser beam passing through this grating will be diffracted into several different orders. It's angular deviation is linearly proportional to the acoustic frequency, so that the higher the frequency, the larger the diffraction angle Θ:

$$\Theta = \frac{\lambda \cdot f_a}{v_a} \qquad (6.1)$$

where λ is the laser wavelength in air, f_a is the acoustic frequency and v_a is the acoustic velocity. With acousto-optic modulators both deflection as well as modulation of the beam amplitude are possible. Also, in the acousto-optic interaction, the laser beam frequency is shifted by an amount equal to the acoustic frequency due to phonon absorption. Positive in the 1st order and negative in the -1st order of diffraction. The positive shift is equivalent to a doppler shift of the light that occurs when the light is diffracted off the moving grating. In my experiments two *ISOMET 1205C* acousto-optic modulators have been used, powered by an *ISOMET D320* AOM driver.

23

6.3 Signal detection

RCA Tube Operations, *RCA C31034* 51 *mm* diameter photomultiplier tube with a gallium arsenide photocathode.

Hamamatsu, *S1223* Two identical silicon PIN photodiodes with a bandwidth of 30 *MHz*. Used with double-shielded matched coaxial cables.

6.4 Electronics

Stanford Research Systems, *SRS DG535* Four-channel digital delay/pulse generator.

Stanford Research Systems, *SRS DS345* 3 *MHz* digital arbitrary waveform generator.

Hewlett Packard, *HP 8013B* Delay/pulse generator.

Hewlett Packard, *HP 8003A* Pulse generator.

Tektronix, *TEK TDS540* Four-channel digitizing 1 *Gs/s* oscilloscope.

Tektronix, *TEK FG504* 40 *MHz* function generator.

FLUKE, *model 412B* High-voltage power supply.

Mascot, *model 719* Power supply.

New Focus, *model 3211* High-voltage ×40 amplifier (max 200 *V*).

Behlke, *HTS31, HTS51* High-voltage switches. Modified with extra HV-protecting diodes and connected as in Figure 6.3 to switch voltages of ±2 *kV*.

Relay shutters Two opaque mechanical shutters.

Low-voltage amplifier Amplification of ×1 − ×3.

High-voltage transformer Increases the voltage 11, 2 times.

Quadruple high-speed amplifier

High-voltage power supply Delivers high-voltage to the *RCA C31034* PMT.

Analogue five-channel signal adder

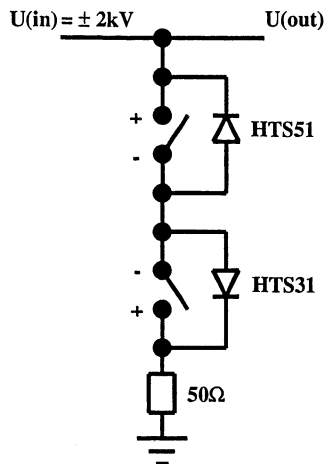*Quadruple analogue switch* Four sets of low-voltage analogue switches.

Figure 6.3: Two HV-switches connected and modified to handle ± 2 kV.

6.5 The cryostat

In order to get the narrow absorption linewidths that we need, the crystal must be cooled in a cryostat to prevent thermal phonons. The cryostat is a *Cryo Vac 150* and can most simply be described as a big thermos with an additional thermos inside. Inside the inner tank the crystal is placed in a bath of liquid helium. Surrounding this tank is a vacuum chamber surrounded by a compartment filled with liquid nitrogen. The space between the outer two layers of the cryostat is another vacuum compartment. The cryostat gives optical access to the crystal and a laser beam can be directed through the crystal and cryostat. This construction makes temperatures around 4 K possible. Connected to the cryostat is a gas evacuation pump. If this is used to lower the pressure on the helium, the temperature can be lowered even further to below 2 K.

6.6 The crystal holder

In order to manoeuvre the crystal from outside the cryostat and enable an electric field to be applied, a special crystal holder had to be designed. Put in this holder, the crystal can be rotated around the propagation axis of the incoming laser light, see Figure 6.4. In order to make this useful, the electrodes generating the E-field are fixed with respect to the cryostat during the crystal rotation. The electrodes are also constructed to generate a homogeneous E-field, making experimental data easier to analyse. As material for the crystal holder the plastic *Delrin* was chosen. It has well known low-temperature and electrical properties.

6.7 The $Eu^{3+}: YAlO_3$ crystal

For all the experiments in this report the same crystal was used. As mentioned in Chapter 3 the material is the rare-earth element europium doped into $YAlO_3$
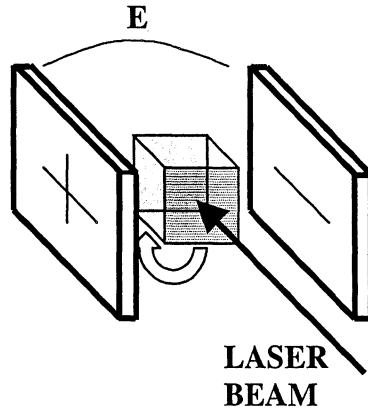
Figure 6.4: The principles of the crystal holder. The crystal can be rotated around the laser light propagation axis with respect to the electrodes.

with a concentration of $0,25$ %, where yttrium is substituted. This combination has been selected basically for four reasons

- long coherence time

- long hyperfine level lifetimes

- a suitable hyperfine splitting for qubit construction

- combination of large inhomogeneous and small homogeneous absorption broadening

The dimensions of the crystal are $5 \times 5 \times 5$ mm and it is colorless for the eye. The energy levels used are the $^7F_0$ and $^5D_0$ of Eu^{3+}. Despite the fact that $J = 0$ for these states, they are both split into three doubly degenerate hyperfine levels. This is an effect of lattice imperfections in the $YAlO_3$ crystal. The imperfections cause a gradient in the crystal field affecting the asymmetric nuclei of the europium ions, which then will have different potential energy in different directions (see Figure 6.5). The nucleus of Eu^{3+} in $YAlO_3$ is not
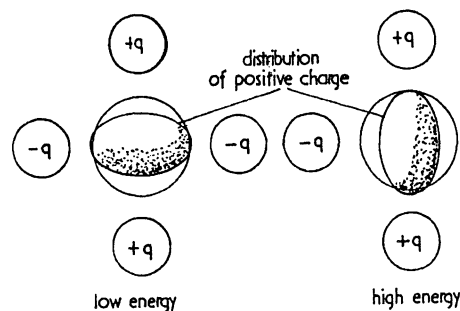
Figure 6.5: A nucleus with assymetric charge density will obtain different potential in different directions with respect to an electric field gradient.

	$^7F_0$	$^5D_0$
^{151}Eu	45,99	89
	23,03	61
^{153}Eu	119,20	226
	59,65	156

Table 6.1: Hyperfine splittings in MHz of Eu^{3+} in $YAlO_3$, from [17]

$a = 0,5329\,nm$	$\alpha = 89,96°$
$b = 0,7370\,nm$	$\beta = 90,00°$
$c = 0,5179\,nm$	$\gamma = 90,02°$

Table 6.2: Lattice parameters of $Eu^{3+}: YAlO_3$, from [18]

spherical, but symmetric around its spin axis. If the spin of a nucleus is large, $I > 1/2$, it has a quadrupole moment and it can obtain either the shape of a cigarr or the shape of a discus. In the field gradient of the crystal, caused by lattice imperfections, the Eu^{3+} nucleus can be oriented in $(2I + 1)$ directions, resulting in six energy eigenstates[1], where I is the nuclear spin of $5/2$. The nuclear spin directions corresponding to I_z and $-I_z$ will obtain the same potential energy in the gradient field, resulting in only three doubly degenerate energy levels ($I_z = \pm1/2, \pm3/2, \pm5/2$). This *quadrupole interaction* is not the only mechanism describing the level splittings. The levels are also affected by a second order hyperfine interaction. Thus the energy levels are still called hyperfine levels, even though $J = 0$. The $^7F_0 \longleftrightarrow ^5D_0$ transition used is not allowed by the standard selection rules. The deviation from these rules is made possible through a natural mixing of the $^7F_0$ state with manifolds with higher J-values.

Natural Eu has two different isotopes, $^{151}Eu(44,8\ \%)$ and $^{153}Eu(52,3\ \%)$, with the same $^7F_0 \longleftrightarrow ^5D_0$ transition frequency of $581,68\ nm$. One thing that differs between the isotopes are the hyperfine splittings. This will result in double sets of side-holes and anti-holes during holeburning experiments. For the experiments conducted in this report this does not have a great influence. The energy structure of the hyperfine splitting can be seen in Table 6.1. The crystal of $Eu^{3+}: YAlO_3$ has a distorted orthorhombic[2] structure with the lattice parameters in Table 6.2.

---

[1]The levels are said to be quadrupole split

[2]Distorted orthorhombic structure can be seen as a tilted cube

Chapter 7

SMPE experiments

As mentioned in section 3.2.1 the difference in permanent dipole moment between the ground and excited state in $Eu^{3+} : YAlO_3$ can have four different directions, this is visualised in Figure 3.4. To benifit from this knowledge one needs to know these directions relative an external applied electric field, i.e. relative the sides of the crystal surfaces. We accomplished this by using Stark-modulated photon echoes (*SMPE*). As described in section 4.2, interfering echoes will be created if an electric field is applied between the first and second pulse in a photon echo measurement. This is under the condition that the photon echo material contains groups of atoms receiving different amounts of energy (positive or negative) in the electric field. In our crystal only one modulation frequency will occur if the E-field is applied in any of the two directions shown in Figure 7.1. This would help us to pinpoint the directions of the dipole moments. Several other directions of the E-field were used and the resulting modulations were registered.
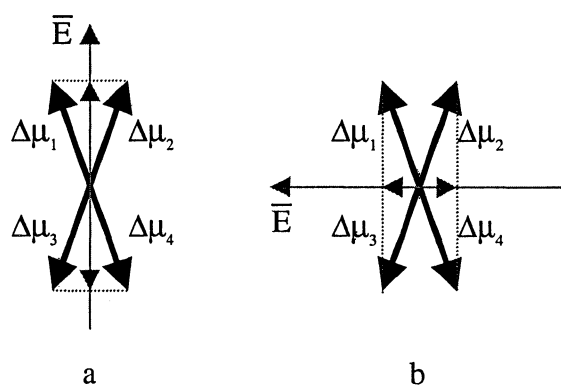
Figure 7.1: If the E-field $\bar{E}$ is applied as in case **a**, the modulation frequency will be higher than in case **b**. This is due to larger difference in the resulting energy shifts which are equal to $\Delta\mu \cdot \bar{E}$.

7.1 Experimental set-up

To create the laser pulses needed for this 2PPE experiment we used two AOMs in series. Two were needed to reduce the light "leaking" through the set-up to the crystal when the AOMs were turned off. AOMs don't have as good on-off ratio as mechanical shutters, but the advantages are large. The AOMs are several orders of magnitude faster than mechanical shutters and they don't induce any vibrations into the set-up. When the AOMs were activated they diffracted the incoming laser light. The first order diffraction was then let through an aperture as in Figure 7.2. In this way the light could be turned on and off.

To switch the electric field on and off ($0\ V - 200\ V$) and to control its duration, a computer was utilised. The computer also triggered the AOMs.

A single photodiode was used to detect the echo signal. The detection was gated by the computer, only to register the echo signal. With the help of the computer an averaging over 256 shots could be made for every value of the E-field duration.

In order to rotate the crystal with respect to the electric field, the crystal holder briefly described in section 6.6 was used. This made the crystal somewhat controllable. For simplicity all devices for the pulse generation and most of the control electronics are left out of the figures descibing the different set-ups in the report. This reduces the number of "boxes" in the figures by $10 - 15$ in some cases.
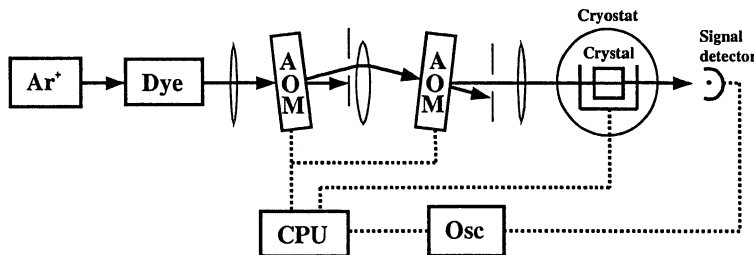

Figure 7.2: Eperimental set-up: Stark-modulated photon echoes. The Ar ......er pumping the dye-laser will be used in all experiments.

7.2 Results and discussion

Stark-modulated photon echoes were registered with E-field durations τ_E between $0,5\ \mu s - 5\ \mu s$. For technical reasons τ_E could not be set to a lower value than $0,5\ \mu s$. Similar recordings were conducted for different angles of the E-field with respect to the crystal. Since the resulting echo modulations are repeated four times for every full turn, $360°$, of the E-field, only five recordings from the first $180°$ are presented in Figure 7.4.

A simulation of the modulations was also carried out. The model used is the following, taken from [19]:

$$I_{modulation} = |C_{12}e^{i\Omega_{12}\tau_E} + C_{13}e^{i\Omega_{13}\tau_E} + C_{14}e^{i\Omega_{14}\tau_E} + C_{24}e^{i\Omega_{24}\tau_E}|^2 \cdot e^{-\alpha\tau_E} \quad (7.1)$$

where Ω_{ij} is the frequency corresponding to the energy difference between ions with dipole moments $\Delta\mu_i$ and $\Delta\mu_j$. Due to symmetry there will only be four different frequencies in each modulation. The exponential decay of the modulation intensity originates from inhomogenities in the electric field in the crystal. In Figure 7.3 the echo modulation with the E-field applied at $0°$, as in Figure 7.1(a), is compared to the simulated counterpart. As can be seen in Figure 7.3
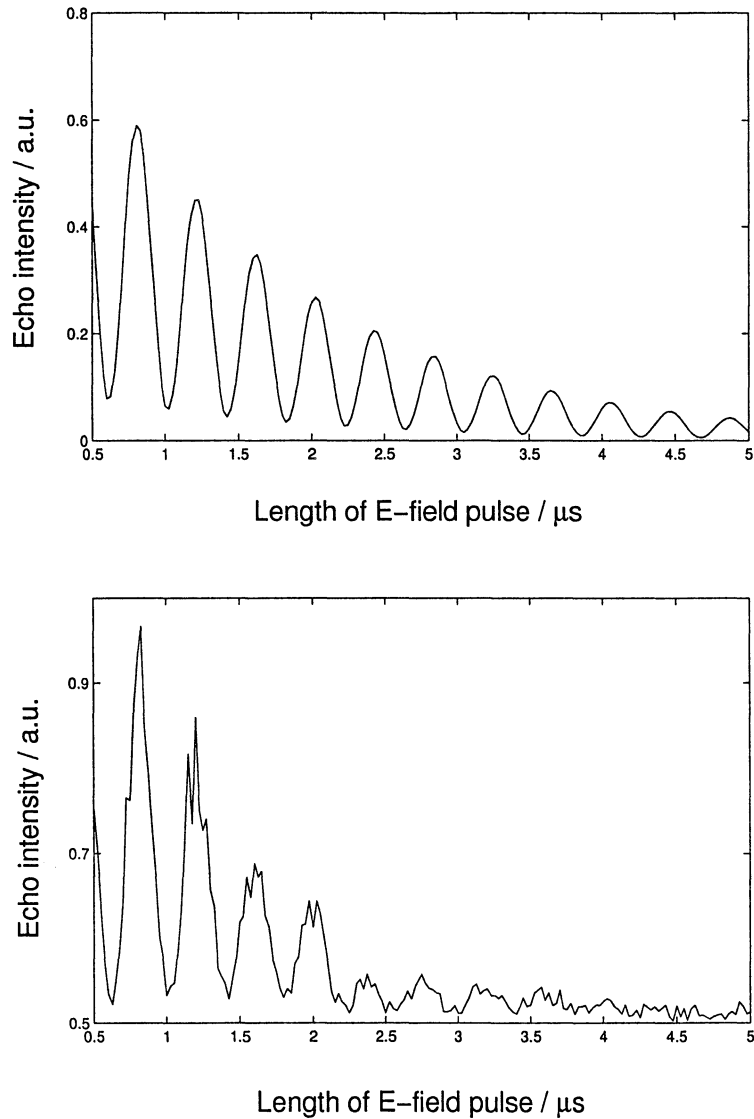

Figure 7.3: A simulated echo modulation (top) with an E-field angle of $0°$ with respect to the crystal and the experimental counterpart (bottom).

the detected modulation truly is sinusoidal, as predicted in section 4.2.

From the data presented in Figure 7.4 the directions of the dipole moments with respect to the crystal surfaces can now be calculated. The angle precision

is somewhat moderate though. The rotation of the crystal could only be set with a $10° - 15°$ accuracy due to mechanical limitations. But since the direction of the E-field corresponding to the slowest modulation seemed to be parallel to the crystal sides, we are reasonably confident that the crystal is cut this way intentionally.
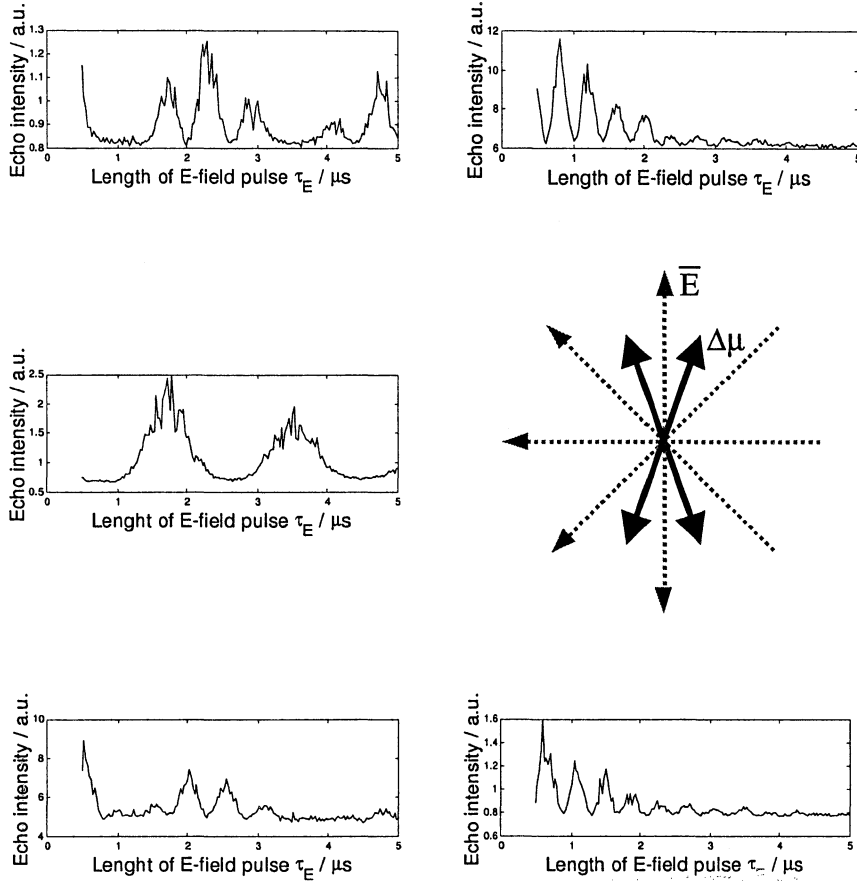

Figure 7.4: The resulting echo modulations for five different directions of an applied electric field with respect to the dipole moment directions.

31

Chapter 8

Holeburning and holesplitting experiments

In order to learn more about the absorption properties of the crystal with the use of holeburning and to study how the holestructures respond to the application of electric fields the following experiments were conducted.

8.1 Experimental set-up

The basic stucture of this set-up was the same as in the SMPE experiments in Chapter 7. The two AOMs were still used to modulate the laser intensity, but they had an additional function in this experiment. If the frequency of the acoustic wave in an AOM is varied, the frequency of the deflected light is also varied by an equal amount. Positive in the 1st order and negative in the -1st order of diffraction. When two AOMs are set up as in this experiment their frequency shifts will be added, generating a maximal frequency tuning range of approximately 80 MHz. The combination of lenses, shown in Figure 8.1, prevents the laser beam from changing direction. The frequency tuning is generated with the arbitrary waveform generator *SRS DS345*, which can be programmed via a PC (CPU in Figure 8.1). After a spectral hole was created we probed the absorption profile by first reducing the laser light intensity with the AOMs by a factor of 50, not to ruin the hole structure, and then scanning the frequency with the AOMs.

In these experiments we did not want to record averages over a large amount of pulse series, instead we wanted single-shot results. To do this we increased the signal-to-noise ratio considerably by using two matched photodiodes for signal detection. One diode registering the signal through the crystal and the other registering an unaffected reference signal. The arrangement is shown in Figure 8.1. By dividing the first signal by the reference, much smaller structures could be detected than before. Power fluctuations in the laser and electrical disturbances were almost completely removed from the resulting signal in this way.

To generate an electric field for the holesplitting experiments a powerful *FLUKE 412B* high voltage supply was used. Voltages between 0 V − 2 000 V were applied to the crystal electrodes.
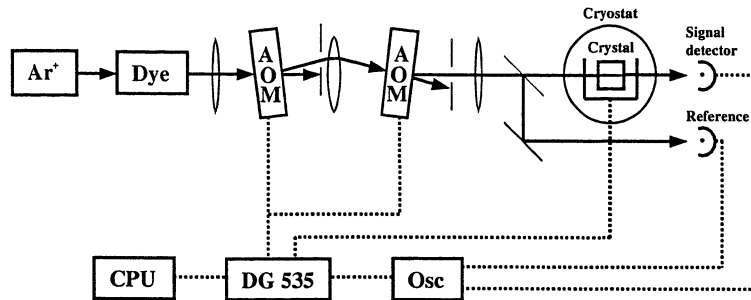
Figure 8.1: Experimental set-up: Holeburning. The whole experiment was triggered by the $SRSDG535$ delay generator. This also provided the AOMs with on-off pulses.

8.2 Results and discussion

When a single hole is burnt in the absorption profile, one can automatically measure the linewidth and frequency stability of the laser used. Every spectral channel in the crystal is a few kHz wide in frequency, so the width of the hole in Figure 8.2 is only due to the broader linewidth of the laser and its frequency drift in time. Apparently these two effects in this case added up to an effective linewidth of $1,5\ MHz$ FWHM[1] when the hole was burnt for 100 ms. This can be treated as a fairly good result since a typical result for burn times of hundreds of milliseconds typically is $2\ MHz - 3\ MHz$ according to the rest of our results. The longer the hole is burnt the more the laser generally drifts, resulting in a widened hole. When the crystal was affected by an electric field of about 15 V/cm the hole in Figure 8.2 was clearly widened and got less deep. To observe a splitting of the hole we applied voltages between $0\ V - 1\,000\ V$ over the crystal electrodes[2]. The experiment was successful and the detected signal from the splitted hole is presented in Figure 8.3 and Figure 8.4. When voltages above $1\,000\ V$ were applied the holes got fainter and wider due to field inhomogenities in the crystal. If the crystal was to be tilted from this $0°$ position relat⁻ ⁻ the E-field, the splitted hole would have gotten four components. This was also experimentally verified in my project. The data is not submitted in this report since the signal-to-noice ration was very bad for that particular experiment.

---

[1]Full width at half maximum

[2]Approximately 15 % of the voltage is applied to the crystal, the rest is "lost" over the crystal holder.
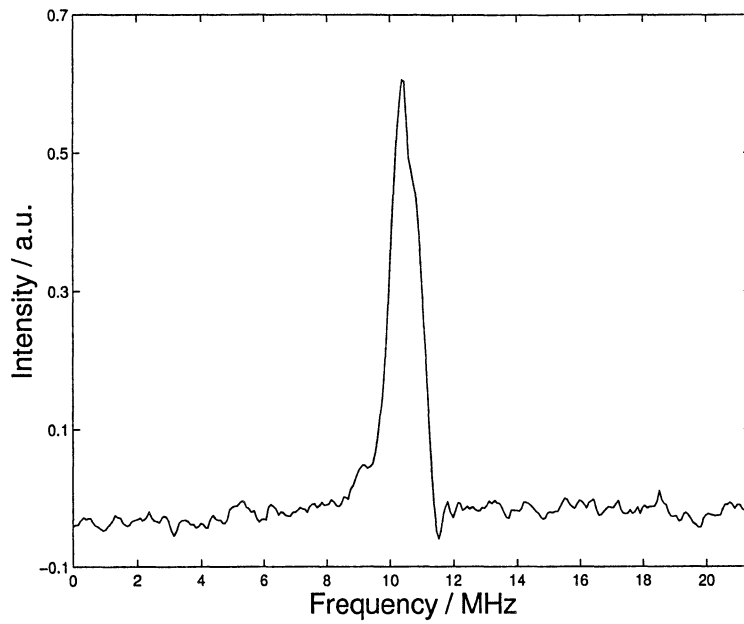
Figure 8.2: The transmission through the crystal when scanning the absorption profile over a hole burnt for 100 *ms*.
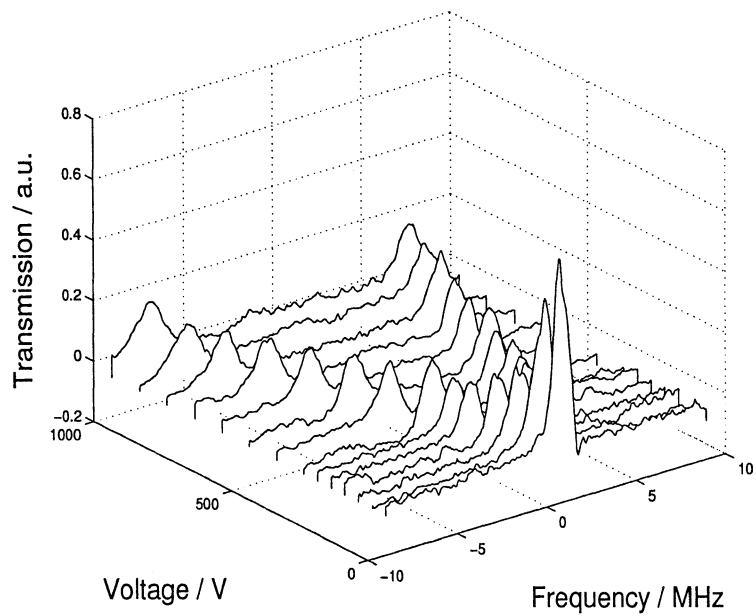

Figure 8.3: A hole split in two components when affected by an increasing electric field. The voltage is the one applied to the electrodes, approximately 15 % of this falls over the 5 *mm* wide crystal. The hole was probed using transmission measurements.
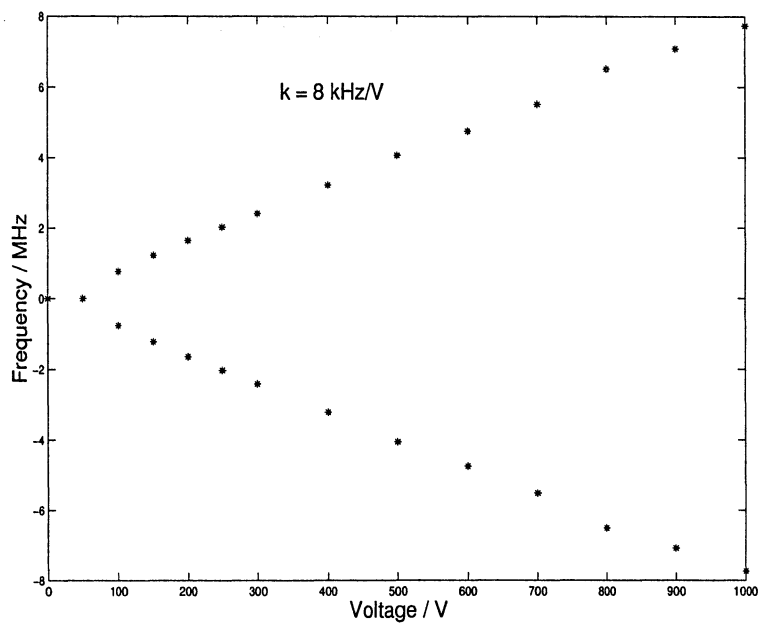
Figure 8.4: A hole split in two components when affected by an increasing electric field voltage. The location of the bottom of the hole is plotted.

Chapter 9

Experiments for detecting dipole-dipole induced ion interaction

The main aim of my project was to detect dipole-dipole interaction between ions in $Eu^{3+} : YAlO_3$. We tried to observe this by studying the change of a spectral hole when ions with dipole moments in a specific direction were excited. This selective excitation should make the interaction effects larger than if both directions were to be excited. Since the electric field used in this experiment was applied as in Figure 7.1(a), ions with the same projection on $\bar{E}$ would gain the same energy shifts and the ions can then be divided into two groups based on the orientation of their dipole moments instead of four. Selective excitation of one of these groups was accomplished in two different ways, methods I and II.

9.1 Selective excitation

9.1.1 Method I

The first method (I) was based on what happens when a wide hole is shifted by an electric field. As shown in Figure 9.1 ions of the two groups would shift in different directions, creating two areas in the absorption profile where the groups are isolated. If one of these groups now was excited, the hole would become wider (if the left region was to be excited) or more narrow (if the right region was to be excited), depending on whether the induced electric field from the excited ions is directed against or along the applied field respectively.

9.1.2 Method II

The second method (II) was technically more advanced than method I. It was designed to overcome a weakness of the first method, namely the limited frequency interval available for selective excitation[1]. To solve this two different

---

[1] The interaction is expected to be stronger the more ions that are excited.
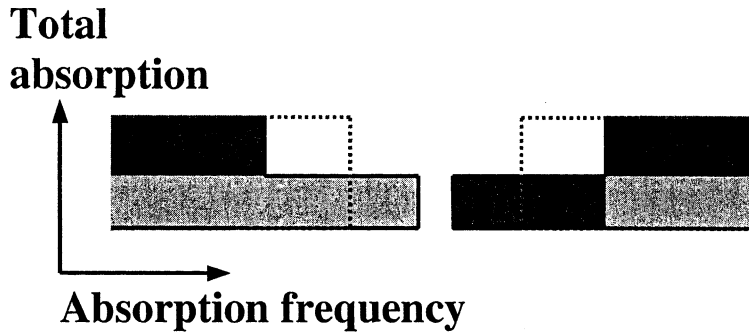
Total absorption

Absorption frequency

Figure 9.1: When a spectral well is shifted by an applied electric field and two different groups of ions are present (represented by different colors), two areas are created with only one group of ions in each. The dotted line represents the unperturbed well.

holes were burned. One was used as an inspection hole which was monitored in order to look for frequency shifts and the other provided a "window" in the absorption profile. This window was used to selectively excite one of the groups of ions. When a hole is split into two components by an electric field (see Figure 5.3) and the laser is tuned to one of these holes the absorption at the hole frequency is due to ions from one group only. In this way a hole component serves as a "window" in the absorption profile and allows you to access ions from one group separately. By continously increasing an electric field applied to the crystal, the frequency separation of the holes will continously increase. By tuning the laser excitation frequency we followed one of the components of the window. Selective excitation of one group of ions was accomplished over a large frequency interval. To take advantage of the wider frequency interval and the correspondingly larger number of ions excited, the excitation and read-out of the inspection hole had to be done within the lifetime of the excited state ($\approx 2\ ms$). The electric field was varied within a 4 kV interval and to prevent current discharges in the cryostat we had to use voltages between $-2\ kV$ and $+2\ kV$. With the knowledge gathered in the holesplitting experiments we used a separation between the two holes in this experiment of at least 32 MHz at zero field. If they were located closer in frequency one of the two components of the inspection hole would have the same frequency as the window in which we excite for some electric field (see Figure 9.2). This would not make a very good experiment since the effects of any ion-ion interaction and hole deformation due to excitation never could be separated. Method II enables a maximal selective excitation interval of 64 MHz versus 5 $MHz - 10\ MHz$ for method I. The frequency interval in method I is limited by the width of the areas in Figure 9.1 containing only one group of ions.

To improve the signal-to-noise ration of method II we lowered the pressure in the cryostat, thus lowering the temperature of the helium to the λ-point where the helium becomes superfluid. This means that no bubbles are created in the helium and disturbance and scattering effects of the laser light are reduced.
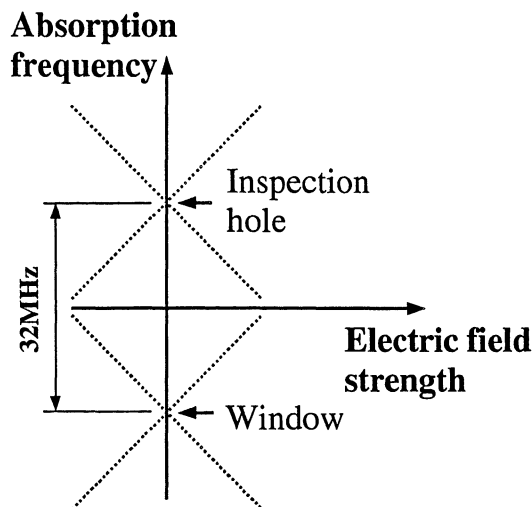
Figure 9.2: When two spectral holes are burned and affected by an applied electric field, two of the splitted components of the holes will at som voltage have the same absorption frequency.

9.2 Experimental set-up

In this experimental set-up, Figure 9.3, we alternated between two different detection systems. We used a photomultiplier tube (PMT) to investigate the created structures needed for the excitation experiments. The PMT has the advantage of low noise levels and superior amplitude sensitivity to photodiodes. Thanks to this high sensitivity we could detect the fluorescence signal from the crystal instead of the transmitted laser light, retrieving an absolute zero-level when off-resonance to compare the depths of the holes to. As a minus a PMT is less convenient to work with and we only had one of them, so we couldn't divide the signal by a reference. Because of this the created structures were also investigated using the two matched photodiodes as the detection system.

The equipment generating the electric field in method I was the same *FLUKE 412B* power supply as in the holesplitting experiments connected to a high-voltage switch, enabling automatic on-off switching of the field.

For method II the system needed to be more versatile. It had to be able to tune the voltage over the crystal holder electrodes between $+2$ kV and -2 kV and back to exactly 0 V before the inspection hole could be read out. All this has to be done within 1 ms, i.e. before the excited ions have had the time to decay to the ground state. Especially the step back to 0 V proved to be hard to do without causing severe voltage transients in the system. The requirements could finally be met when we used the two connected HV-switches in Figure 6.3 to short-circuit the voltage to ground.

The frequency tuning of the laser light was also more complicated for method II than described before. We had to be sure the frequency of the laser light was positioned within one of the electric field tuned window components during the whole excitation process. To accomplish this we had to feed the high-voltage amplifier components with the same signal as was fed to the frequency modu-

lation of the AOMs. Before the signal reached the amplifiers though we filtered out everything but the part representing the $+2\ kV$ to $-2\ kV$ sweep in the signal with a low-voltage switch. The resulting pulse sequences for the amplitude- and frequency modulation of the AOMs and the signal to be amplified by the HV-components can be seen in Figure 9.4.
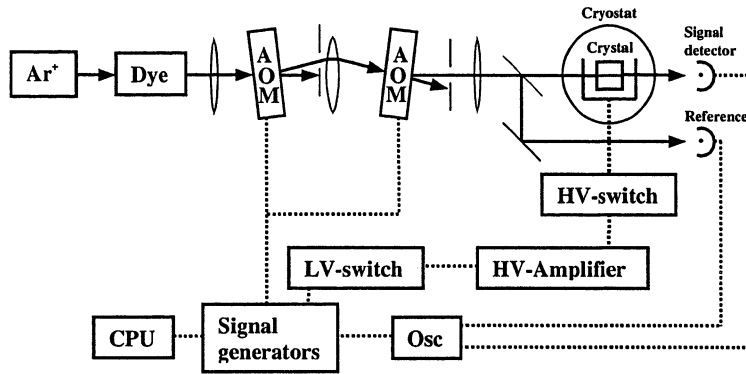

Figure 9.3: Experimental set-up: Ion-ion interaction. The whole set-up is triggered by the signal generators. In some of the experiments we used a PMT for detection, instead of the photodiodes. Se Appendix A for the complete set-up.
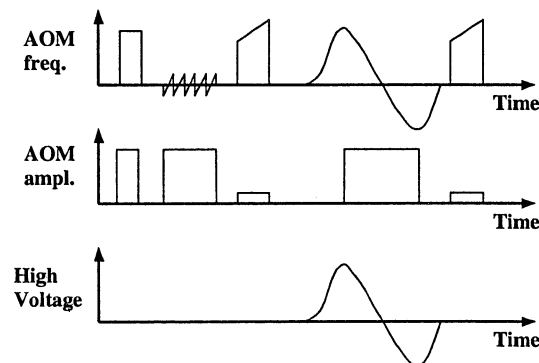
Figure 9.4: The resulting pulsetrain fed to the AOMs, for frequency and amplitude modulation of the laser light, and to the crystal electrodes. The first two pulses to the AOMs burns the inspection hole and window respectively. The third and fifth pulses are for the inspection hole read-outs. The fourth pulse generates the splitting and tracking of the window.

39

9.3 Results

9.3.1 Method I

The structures needed for method I were successfully created. An unperturbed wide spectral hole (a well) at zero electric field and the corresponding structure when an electric field voltage of 700 V is applied to the sample are pictured in figures 9.5 and 9.6. Several sequences of measurements corresponding to method I were gathered and analysed. In Figure 9.7 a recording of a well with 1 000 V applied after the hole is created is shown. In the same figure one can se the same well but after an excitation of a 11 MHz wide interval for 500 μs.

9.3.2 Method II

Method II was carried out with many different combinations of excitation pulse lengths and frequency widths. In figures 9.8, 9.9 and 9.10 three different measurements of detection holes are shown, before and after a 60 MHz wide excitation lasting for 500 μs. This means the exciting laser frequency followed the window as it moved 60 MHz during the entire E-field sweep which took 500 μs to complete.

9.4 Discussion

According to simulations done within the photon echo group the ion-ion interaction in $Eu^{3+}: YAlO_3$ is possibly observable with the techniques used in these experiments. As shown in Figure 3.5 the average shifts should be in the order of 300 kHz in each direction[2] which at least should show up as a widening of the inspection hole used in method II. This is not an easy task to spot though. If the shift had been 1 MHz in each direction we are positive it would be detected.

In neither of the experiments according to methods I and II the ion-ion interaction was observed. In method I we only excited ions within a maximum interval of $\approx$ 10 MHz. With the knowledge from the simulations this would render shifts of about 100 kHz in each direction which are very hard to detect. The reason why the shifts were not seen in the experiments described by method II where we excited ions in an interval of $\approx$ 60 MHz is not clear. In figures 9.8, 9.9 and 9.10 the holes appear to be slightly shifted, but the shifts are not consistent and could therefor not arise from ion-ion interactions. There are several possible explanations to why the interactions were not detected:

- The frequency resolution of the system was to poor due to the linewidth and frequency jitter of the laser.

- There is a possibility we were not exciting as many ions as we expected. We assumed that 50 % of the target ions were excited from the ground state to the excited state. This assumption is based on the facts that we focus the beam with a power of $\approx$ 100 mW in the crystal and experience tells us that should be enough intensity for the excitation. We have no way of checking if this assumption is valid at the moment.

---

[2]In Figure 3.5 only ions with a positive energy shift are shown. The same distribution, although mirrored around 0 MHz, describes the ions with a negative shift.

- The program used to simulate the ion-ion interactions is not designed for the situation when atoms with dipole moments in one direction only are excited. The predictions made can therefor suffer from errors.

- Perhaps a shift was present but is drowned in the natural variations between measurements. With a larger statistical material we could investigate this. In my project this was not carried out.

- The change in electric field induced when a transition is made may be effecting the surrounding Eu ions in a different way than we expected, due to interference with other atoms the $YAlO_3$ crystal.
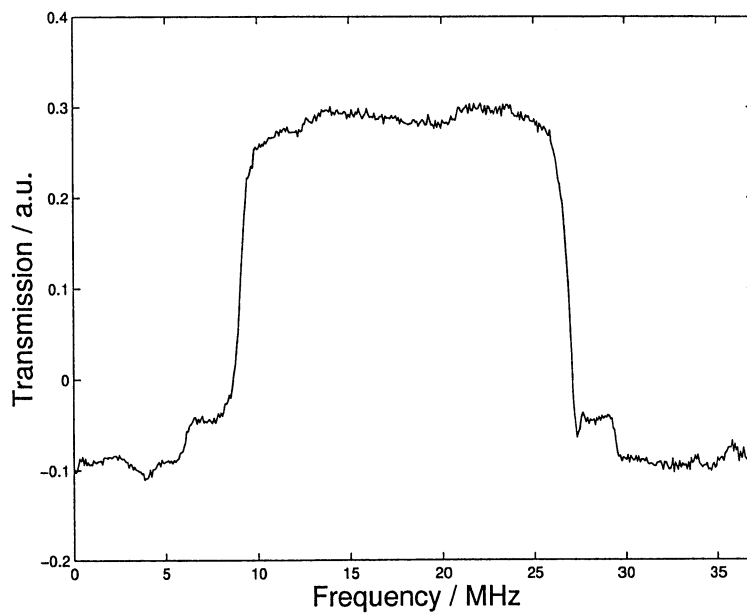
Figure 9.5: An unpertubed well, burnt for 1.5 ms
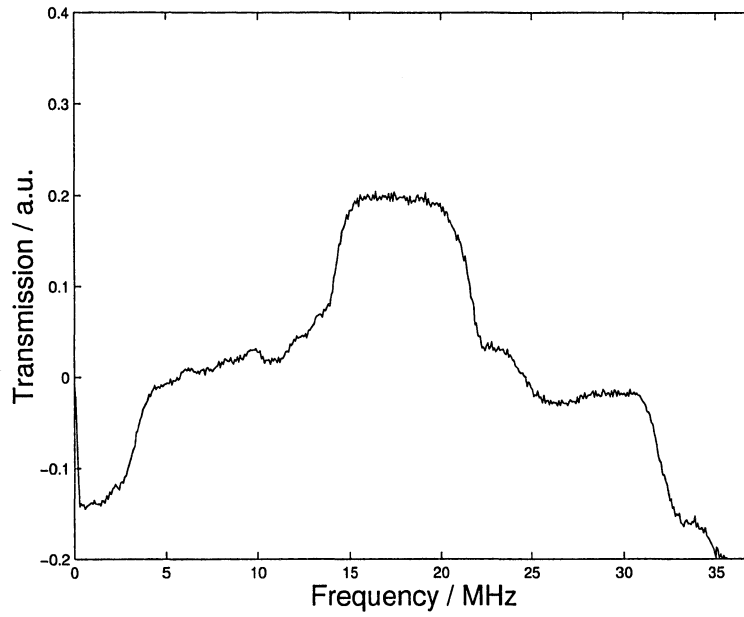
Figure 9.6: A well distorted by an applied voltage of 700 V.
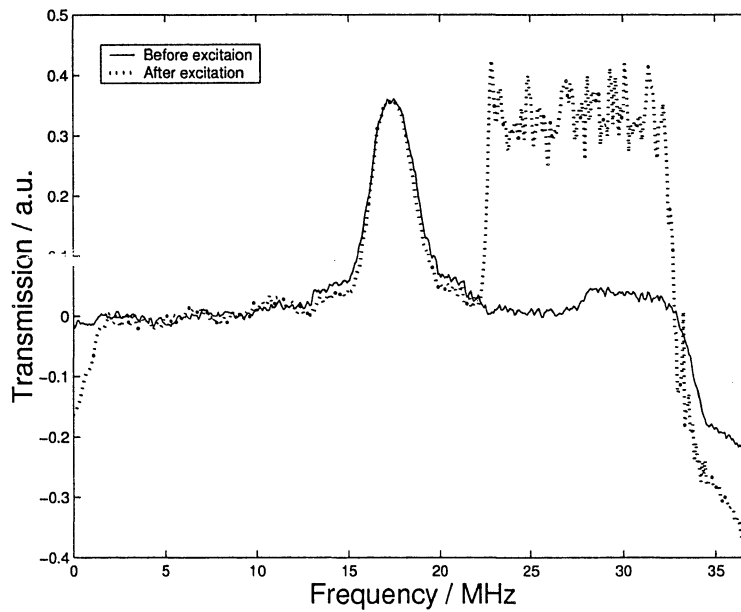
Figure 9.7: A well structure when 1000 V is applied to the crystal holder (solid). The same well after exciting 11 MHz (dotted).
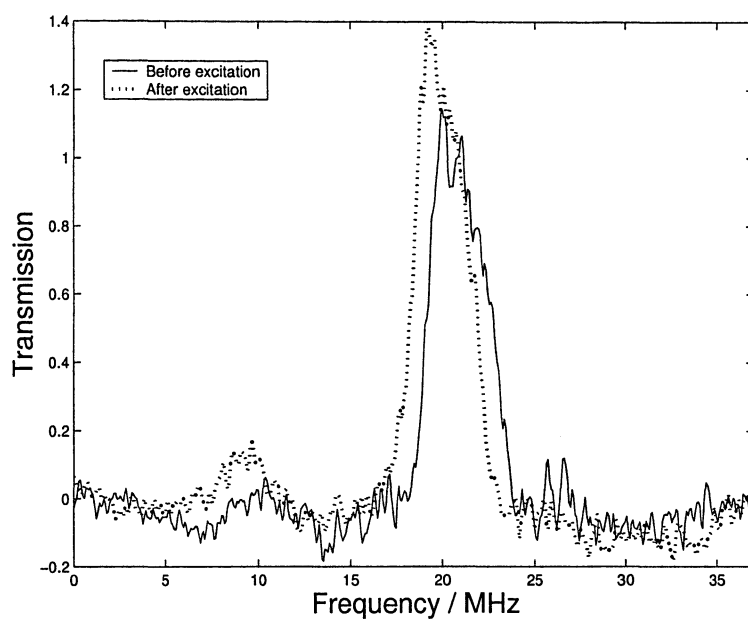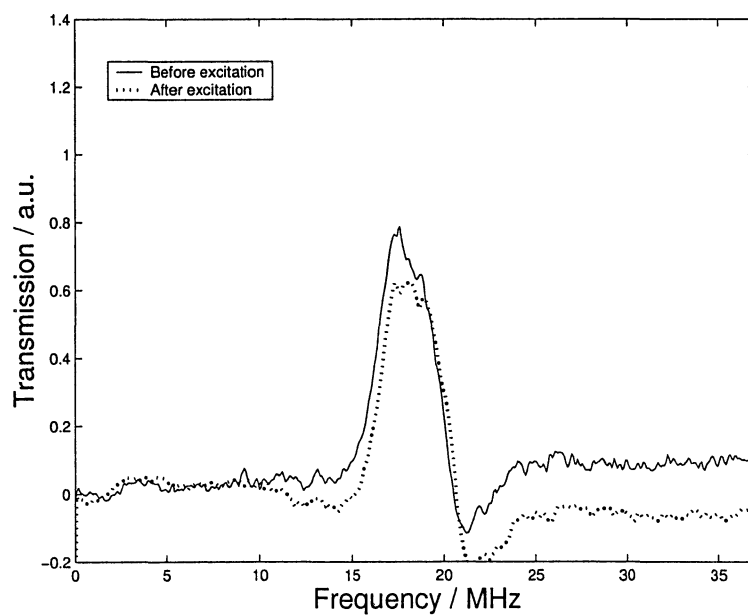
Figure 9.8: A spectral hole burnt for 100 *ms* before (solid) and after (dotted) exciting in the window.

Figure 9.9: A spectral hole burnt for 100 *ms* before (solid) and after (dotted) exciting in the window.
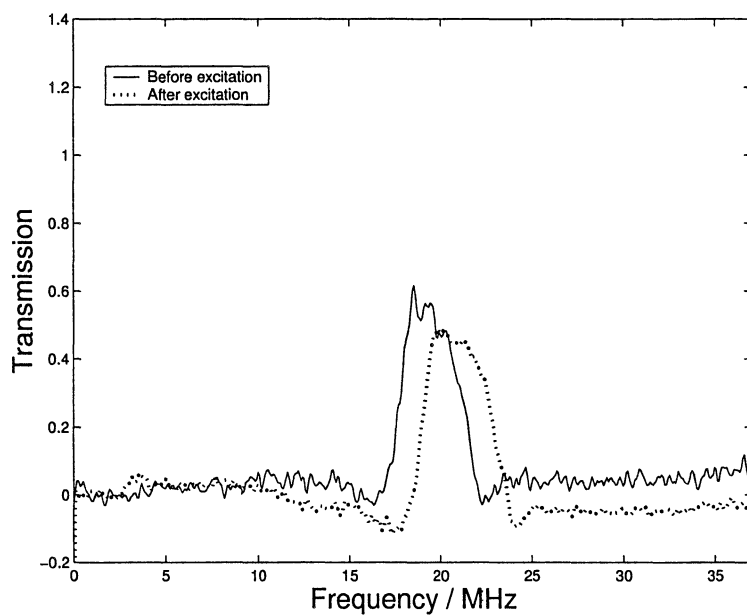
43

Figure 9.10: A spectral hole burnt for 100 *ms* before (solid) and after (dotted) exciting in the window.

Chapter 10

Conclusion

In order to realise the quantum computer operations described in section 3.3.2 and the scheme for a quantum computer based on $Eu^{3+}:YAlO_3$ developed in the photon echo group, the ion-ion interactions have to be studied further. The interaction has to be large enough for the different qubits to control each other. Without this effect the present scheme can't be used. We were not capable of detecting this effect in any of the experiments conducted in my project.

The Stark-modulated photon echo experiments shows us that different crystal properties (dipole moment directions, energy shifts etc.) can be investigated and measured in a very fascinating way. If the magnitude of an applied electric field inside the crystal is well known, the energy shifts originating from it can be measured very accurately with this technique.

The series of holeburning- and holesplitting experiments have given us a qualitative feel for how the different ions behave in strong applied electric fields. This makes it easier to anticipate what degree of complicated structures one can create in the absorption profile in future experiments.

10.1 Possible improvements

A way to improve the results of the experiments designed to detect the ion-ion interaction is to enhance the frequency resolution of the system. This could be done by stabilising the frequency jitter of the dye laser. This stabilisation is currently handled within the group by diploma worker Robert Saers.

A sure way to make the ion-ion interaction more clear is to excite a larger frequency interval in the absorption profile, i.e. a larger number of europium ions. Another way is to increase the concentration of europium ions in the crystal. This will make the europium ions sit closer in the crystal lattice and the interacting effects should be stronger.

There is nothing saying $Eu^{3+}:YAlO_3$ is the best system to use. There could be other candidates, undiscovered by us. If europium is changed to praseodymium, another rare-earth element, the ion-ion interaction may be stronger. Experiments indicating this are presently conducted in our group. A downside to this is that praseodymium is not as suitable for the quantum computer scheme as europium.

Acknowledgements

Bibliography

[1] G. Berman, G.D. Doolen, R. Mainieri, V.T. Tsifrinovich, *Introduction to Quantum Computers*, World Scientific Publishing, (1998).

[2] D. Bouwmeester, A. Ekert, A. Zeilinger, *The Physics of Quantum Information*, Springer-Verlag, (2000).

[3] P.W. Shor, *Polynomial-time algorithms for prime factorization and discrete logarithms on a quantum computer*, Proc. 35th Annual symposium on Foundations of Computer Science, (1994).

[4] L.K. Grover, *A fast quantum mechanical algorithm for database search*, ACM symposium on Theory of Computing, (1996).

[5] E. Knill, R. Laflamme, R. Martinez, C-H. Tseng, *An algorithmic benchmark for quantum information processing*, Nature **404**, 368 (2000).

[6] S. Svanberg, *Atomic and Molecular Spectroscopy*, 3rd ed., Springer-Verlag, (2001).

[7] A. Barenco, D. Deutsch, A. Ekert, *Conditional Quantum Dynamics and Logic Gates*, Physical Review Letters **74**, 4083 (1995).

[8] C. Cohen-Tannoudji, B. Diu, F. Laloë, *Quantum Mechanics*, John Wiley & Sons. (1992).

[9] N. Ohlsson, R.K. Mohan, S. Kröll, *Quantum Computer Hardware based on Rare-earth-ion doped Inorganic Crystals*, accepted for publication in Optics Communication, (2001).

[10] R.M. Macfarlane, R.M. Shelby, *Coherent Transient and Holeburning Spectroscopy of Rare Earth Ions in Solids*, Spectroscopy of Solids, (1987).

[11] R. Yano, M. Mitsunaga, N. Uesugi, *Stimulated-photon-echo spectroscopy. I*, Physical Review B **45**, 12752 (1992).

[12] M. Yamaguchi, K. Koyama, T. Suemoto, M. Mitsunaga, *Perturbed ion sites in $Eu^{3+} : YAlO_3$ studied by optical-rf double-resonance spectroscopy*, Physical Review B **59**, 9126 (1999).

[13] A.J. Meixner, C.M. Jefferson, R.M. Macfarlane, *Measurement of Stark effect with subhomogeneous linewidth resolution in $Eu^{3+} : YAlO_3$ with use of photon-echo modulation*, Physical Review B **46**, 5912 (1992).

[14] T. Christiansson, *A first step towards Quantum Computing in Rare-earth-ion-doped crystals*, Lund Reports on Atomic Physics **LRAP-266**, (2001).

[15] H. Hertz, L-Å. Nilsson, *Kontruktion och testning av digital våglängdsmätare*, Master's thesis, Lund Institute of Technology (1980).

[16] Coherent, *699 ring dye laser manual*.

[17] R.M. Shelby, R.M. Macfarlane, *Measurement of the Anomalous Nuclear Magnetic Moment of Trivalent Europium*, Physical Review Letters **1172**, (1981).

[18] S. Geller, E.A. Wood, *Crystallographic Studies of Perovskite-like Compounds*, Acta Crystallography **563**, (1956).

[19] F.R. Graf, *Investigations of spectral dynamics in rare earth ion doped crystals using high resolution laser techniques*, PhD thesis, ETH Zürich (1998).
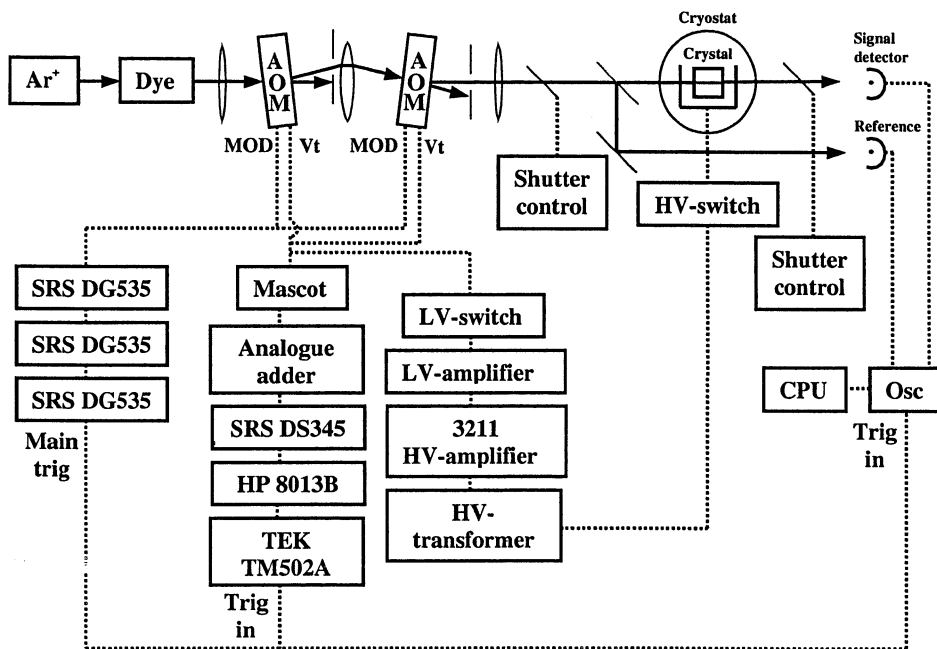
Appendix A

Experimental set-up

Figure A.1: Experimental set-up: Ion-ion interaction. The complete version of the set-up shown in Figure 9.3.